Journal of VLSI Signal Processing 38, 147–156, 2004

Iris Recognition Using Wavelet Features

JAEMIN KIM, SEONGWON CHO AND JINSU CHOI
School of Electronics and Electrical Engineering, Hongik University, 72-1 Sangsu-dong, Mapo-gu Seoul, Korea, 121-791

ROBERT J. MARKS II
Department of Electrical Engineering, University of Washington, Seattle, WA 98195, USA

Received January 13, 2003; Revised July 24, 2003; Accepted November 26, 2003

Abstract. The traditional iris recognition systems require equal high quality human iris images. A cheap image acquisition system has difficulty in capturing equal high quality iris images. This paper describes a new feature representation method for iris recognition robust to noises. The disc-shaped iris image is first convolved with a low pass filter along the radial direction. Then, the radially smoothed iris image is decomposed in the angular direction using a one-dimensional continuous wavelet transform. Each decomposed one-dimensional waveform is approximated by an optimal piecewise linear curve connecting a small set of node points. The set of node points is used as a feature vector. The optimal approximation procedure reduces the feature vector size while maintaining recognition accuracy. The similarity between two iris images is measured by the normalized cross-correlation coefficients between optimal curves. The similarity between two iris images is estimated using mid-frequency bands. The rotation of one-dimensional signals due to the head tilt is estimated using the lowest frequency component. Experimentally we show the proposed method produces superb performance in iris recognition.

Keywords: iris recognition, continuous wavelet transform, feature representation, and curve optimization

1. Introduction

The human iris, visible through the clean cornea as the colored disc inside the eye, is a thin contractile diaphragm composed mostly of connective tissue and smooth muscle fibers. It is attached to the eye's ciliary body and open to the pupil. Human iris patterns are highly distinctive to an individual and the image of an eye can be taken at a distance [1]. The automatic verification of an individual based on the human iris has developed in the last decade [2].

Various iris recognition methods have been proposed for automatic personal identification and verification. Daugman [3] first presented a prototype system for iris recognition. For the feature representation, it makes use of a decomposition derived from the application of a two-dimensional Gabor filter to the iris image pattern. Quantized local phase angles yield the final representation. The similarity measure for feature classification is the Hamming distance between the acquired and data base representations. It reported good performance on a diverse database. Wildes et al. [2] presented another iris recognition system. It decomposes the iris pattern into the multiresolution pyramid layers using a wavelet transform. The quantized differences between adjacent resolution levels yield the final representation. The similarity measure is the normalized correlation between two representations. It reported as good performance as the system of Daugman. Both systems of Daugman and Wildes employ carefully designed image acquisition devices to get equal high quality iris images [2, 4, 5]. The devices minimize the deformation of the iris pattern and acquire the sharp and glare-free iris images under fixed illumination. However,

these demands are not easily satisfied in many field applications.

Cho et al. [6] presented a method using a wavelet sub-image at a low-resolution pyramid level. The neural network is used to classify the extracted feature. However, the sub-image is sensitive to a small shift of a full-resolution iris image in the space domain [7, 8]. Zhu et al. [5] presented a shift-invariant method, which decomposes the iris pattern into multiple bands using a two-dimensional Gabor transform or a wavelet transform. The means and variances of all bands are used for the shift-invariant feature representation. However, the means and variances do not contain much information on the spatial characteristics of the iris texture. This restriction limits the performance. Mallat [9] built a translation-invariant representation from zero-crossings of the full-density wavelet subbands. Boles et al. [10] decompose one-dimensional intensity signals computed on circles in the iris and use zero-crossings of the decomposed signals for the feature representation. This method is reported to be robust to the additive white Gaussian noise. However, the number of zero-crossings can differ among iris image samples of an identical iris due to noises. This method was improved by Roche et al. [4], which assumes that if two samples are acquired from an identical iris, the distances between corresponding pairs of zero-crossing in one sample and another are less than given threshold value. Based on this assumption, the similarity measure is the summation of the binary Hamming distances between corresponding pairs. However, the spurious zero-crossing points can degrade the performance.

A cheap image acquisition system using a fixed focus camera has difficulty in capturing equal high quality iris images. This requires new iris recognition methods robust to noises. In general, a high level of detail is sensitive to noises, while a low level of detail is less sensitive. Some wavelet components of the disc-shaped iris texture, the low frequencies in the radial direction and the low-mid frequencies in the angular direction, contain rich information for iris recognition and in addition are robust to noises. This paper describes a new feature representation method based on these components.

This paper is organized as follows: Section 2 briefly addresses the iris localization and normalization. Section 3 presents a new feature representation method for the iris recognition. Section 4 describes the similarity measure and the classification method used for the iris recognition. Section 5 discusses the comparison of the proposed method with two conventional methods. Section 6 provides the experimental results. Finally, we conclude in Section 7 with a summary of the proposed method.

2. Iris Localization and Normalization

Iris recognition methods require accurate iris localization for successful processing. The visual surface of the iris lies outside the pupil and inside the limbus, the border between the sclera and the iris. In this paper, the acquired image is first segmented into a set of components: pupil, eyelashes, eye, face, and light reflection. Then, the iris boundaries are accurately detected using this information and a well-known parametric shape estimation method [2, 5].

2.1. Eye Segmentation

In the iris image acquisition system using infrared LEDs (light emitting diode), the captured images have an intensity distribution typical of that shown in Fig. 1(a). This intensity distribution can be well represented by a mixture of three Gaussian distribution components: dark, intermediate and bright. The dark component contains the portion of the image corresponding to the pupil and the eyelashes. The intermediate component contains the eye regions including the iris. The bright component contains the face and the light reflection. The density function is expressed as

$$p(x) = \sum_{k=1}^{3} \omega_k f(x \mid m_k, \sigma_k), \tag{1}$$

where x denotes an observation of the data, $f(x \mid m_k, \sigma_k)$ denotes the Gaussian density function, (m_k, σ_k) denote the model parameters, and ω_k denotes the mixing parameters. One common method for solving Gaussian mixture models (GMM) is an expectation-maximization (EM) algorithm [11]. EM is an effective procedure for estimating model parameters when data is incomplete. In the E-step of the EM process, the posterior distribution for the hidden variables is evaluated in order to indicate to which component an observation x belongs. In the M-step, the model parameters, (m_k, σ_k), and the mixing parameters, ω_k, are computed. When the histogram of an image deviates significantly from typical due to glasses and non-uniform illumination, the segmentation based on the estimated parameter can result in poor performance. To alleviate

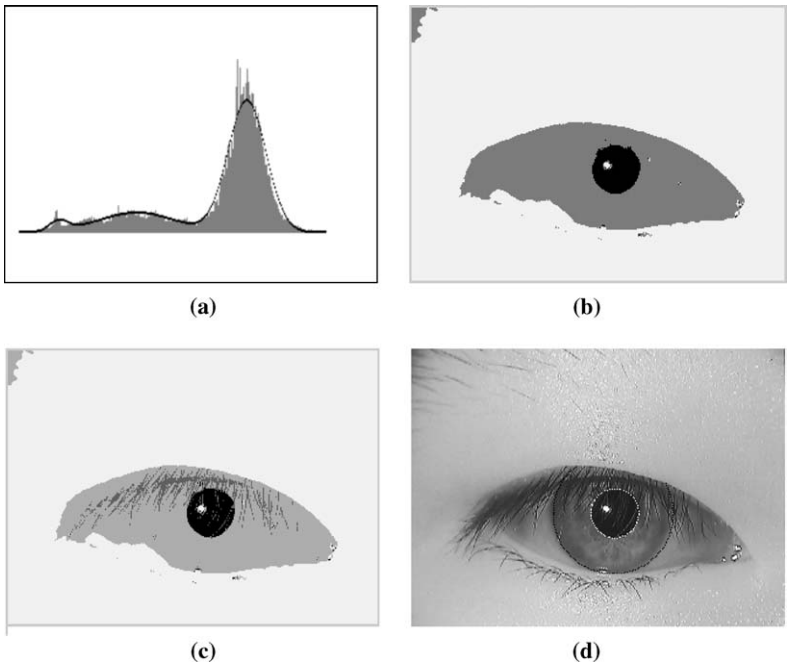

Figure 1. Segmentation results: (a) A typical intensity distribution and its estimation using EM, (b) three segmentation regions processed by a morphological operation with a 5×5 window, (c) eyelashes detected with five directional windows and (d) the detected pupillary and limbic boundaries. The pupillary boundary is indicated by a white dotted line and the limbic boundary is indicated by a black dotted line.

this problem, we project the estimated parameters onto a predefined solution space. The segmentation based on the Gaussian mixture model has segmentation error like a speckle noise because the intensity distributions of three components are overlapped. Such segmentation error is filtered by a morphological operation with a large square window [12]. Since the morphological operation with a large square window filters out the eyelashes, the eyelashes are separately detected using a set of directional long narrow windows. The segmentation results are shown in Fig. 1(b) and (c). Once the iris image is segmented, the iris boundaries are detected using a well-known parametric shape modeling method [2, 5]. The detected iris boundaries are shown in Fig. 1(d).

2.2. *Preprocessing*

Since the acquired iris images have different contrast, the images are enhanced using histogram equalization. The variation of the illumination causes the iris to shrink or to expand. For the iris recognition, it is necessary to compensate the variation of the iris size in the radius direction. A common method is to map the disk-shaped iris to a rectangle block of a fixed size [2]. The rectangle-shaped image, $f(i, j)$, are generated as follows:

$$f(i, j) = f[r_j \cos(\theta_i), r_j \sin(\theta_i)], \quad i = 1, \ldots, N_1, \quad j = 1, \ldots, N_2, \tag{2a}$$

$$\theta_i = i \cdot (\theta_2 - \theta_1)/N_1, \tag{2b}$$

$$r_j = j \cdot \Delta R(\theta_i), \tag{2c}$$

$$\Delta R(\theta_i) = \|l(\theta_i) - p(\theta_i)\|/N_2, \tag{2d}$$

where $f(i, j)$ denotes a two-dimensional intensity signal, θ_i is over $[\theta_1, \theta_2]$, $l(\theta_i)$ denotes a point on the limbus, $p(\theta_i)$ denotes a point on the pupil contour. Figure 2 illustrates trajectories on which $f(i, j)$ is generated.

3. Feature Extraction

In this section, we present a new feature representation method for the iris recognition. The feature representation should have information enough to classify various irises and be less sensitive to noises. In general, a high level of detail of the iris texture is sensitive to noises,

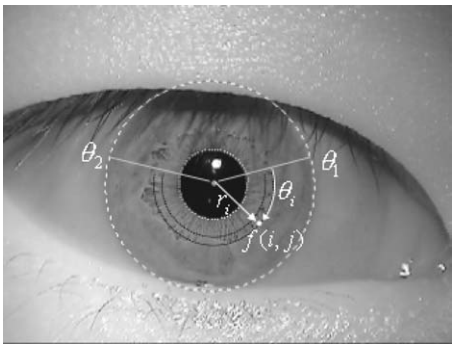

Figure 2. Mapping of the disc-shaped iris to a rectangle block.

while a low level of detail is less sensitive. We have experimentally found that some wavelet components of the iris, the low frequencies in the radial direction and the low-mid frequencies in the angular direction, have rich information for iris recognition and robust to noises.

3.1. Wavelet Decomposition

To extract features from these components, the normalized iris image, $f(i, j)$, is first convolved with a Gaussian low-pass filter along the radial direction, j. The radially smoothed iris image, $g(i, j)$, is decomposed in the angular direction, i, using differences of Gaussian (DoG) like wavelets, the difference of dilated B-splines, $\varphi_{s(k)}(i)$, such that

$$\varphi_{s(k)}(i) = \frac{1}{s(k)}\varphi\left(\frac{i}{s(k)}\right). \tag{3}$$

The smoothing and decomposition procedure is illustrated in Fig. 3. Given a smoothed signal, $g(i, j)$, a set of low-pass filtered signals, $L_{s(k)} * g(i, \cdot)$, is yielded by convolving $g(i, \cdot)$ with $L_{s(k)}(i)$. The difference between two adjacent smoothed signals, $L_{s(k)} * g(i, \cdot)$ and $L_{s(k-1)} * g(i, \cdot)$, forms the k-th band as follows:

$$W_k = L_{s(k)} * g(i, \cdot) - L_{s(k-1)} * g(i, \cdot), \tag{4}$$

where $s(k)$ and $s(k-1)$ are experimentally chosen.

3.2. Generation of the Optimal Piecewise Linear Curve

Once signals are decomposed into multiple bands, each band is approximated by a piecewise linear curve connecting a set of node points. The initial node points correspond to local maximum or minimum points of the band. The initial node points are merged to a small set of node points by iteratively merging two adjacent nodes to the new node point that minimizes the signal distortion. Figure 4 shows that two node points, $\mathbf{v}_k$ and $\mathbf{v}_{k+1}$, are merged to the new node point, $\mathbf{v}_{\text{new}}$, and the piecewise linear curve connecting four node points,

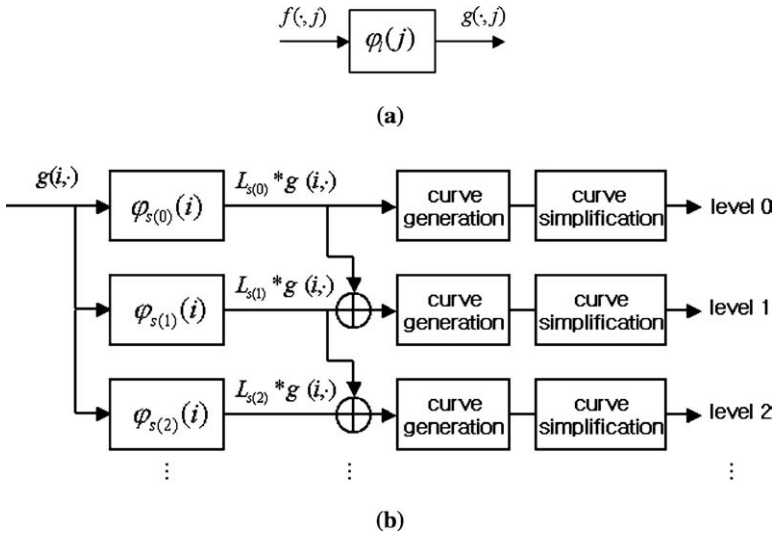

Figure 3. Overall block diagram: (a) The low-pass filtering in the radial direction and (b) wavelet decomposition in the angular direction and the generation of simplified curve.

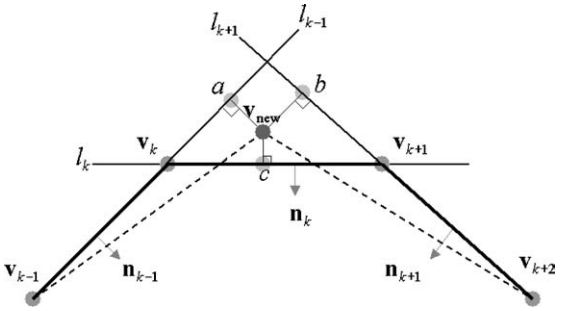

Figure 4. Curve simplification: Two node points $\mathbf{v}_k$ and $\mathbf{v}_{k+1}$, are merged to the new node point $\mathbf{v}_{\text{new}}$, and the piecewise linear curve connecting four node points $\mathbf{v}_{k-1}$,$\mathbf{v}_k$,$\mathbf{v}_{k+1}$, and $\mathbf{v}_{k+2}$, is simplified to the curve connecting three node points $\mathbf{v}_{k-1}$, $\mathbf{v}_{\text{new}}$, and $\mathbf{v}_{k+2}$.

$\mathbf{v}_{k-1}$, $\mathbf{v}_k$, $\mathbf{v}_{k+1}$, and $\mathbf{v}_{k+2}$, is simplified to the curve connecting three node points, $\mathbf{v}_{k-1}$, $\mathbf{v}_{\text{new}}$, and $\mathbf{v}_{k+2}$. In the merging operation, the signal distortion is expressed by three triangles, $\Delta(\mathbf{v}_{k-1}, \mathbf{v}_{k,}\mathbf{v}_{\text{new}})$, $\Delta(\mathbf{v}_k, \mathbf{v}_{k+1,}\mathbf{v}_{\text{new}})$, and $\Delta(\mathbf{v}_{k+1}, \mathbf{v}_{k+2,}\mathbf{v}_{\text{new}})$. If we define the energy of a signal u as $\int u^2(x)dx$, the energy variation of the signal by one triangle, $\Delta(\mathbf{v}_k, \mathbf{v}_{k+1,}\mathbf{v}_{\text{new}})$, is expressed as

$$\frac{1}{3} d_k \left| \mathbf{n}_k \cdot \mathbf{v}_{\text{new}} + c_k \right|^2, \tag{5}$$

where $\mathbf{n}_k$ denotes the normal direction of a line, l_k, connecting two nodes, $\mathbf{v}_k$ and $\mathbf{v}_{k+1}$, d_k denotes the length of the line segment, $\overline{\mathbf{v}_k, \mathbf{v}_{k+1}}$, and $|\mathbf{n}_k \cdot \mathbf{v}_{\text{new}} + c_k|$ represents the distance from the optimal target point $\mathbf{v}_{\text{new}}$ to the line, l_k. The optimal target, which minimizes the energy variation due to the merging operation, is defined as the point that minimize the normalized sum of three energy variation terms:

$$\frac{1}{3E_{\text{total}}} \sum_{i=-1}^{1} d_{k+i} \left| \mathbf{n}_{k+i} \cdot \mathbf{v}_{\text{new}} + c_{k+i} \right|^2. \tag{6}$$

The total signal energy E_{total} is used to normalize the signal distortion. The optimization procedure is performed as follows:

1. Select all node pairs and compute (a) the optimal target for each pair and (b) the cost.
2. Merge the node pair of the least cost to its optimal target.
3. Once a pair is removed, then update the costs of all pairs involving the target of the pair.
4. If the normalized least cost is less than given threshold value, stop the simplification procedure. Otherwise, go to the Step 2.

Figure 5 shows that the simplified curve well approximate the waveform of the signal. The number of the node points of the simplified curve is 20.

4. Classification

4.1. Similarity Measure

The similarity measure for classification is the normalized cross-correlation coefficients between two simplified piecewise linear curves. Each curve is reconstructed using the linear interpolation of a set of node points. The normalized correlation coefficient is given as

$$\overline{\langle \omega\tilde{u}_1, \tilde{u}_2 \rangle} = \frac{\langle \omega\tilde{u}_1 \cdot \tilde{u}_2 \rangle}{\sigma(\omega\tilde{u}_1)\sigma(\tilde{u}_2)}, \tag{7a}$$

$$\langle \omega\tilde{u}_1 \cdot \tilde{u}_2 \rangle = \frac{1}{N} \sum_{i=1}^{N} \omega(i)\tilde{u}_1(i)\tilde{u}_2(i), \tag{7b}$$

where $\tilde{u}_1$, $\tilde{u}_2$ are the zero mean signal, $\langle \cdot \rangle$ is the inner product operator, σ is the standard deviation, and N is the number of points used for computing the correlation coefficient.

In a frequency band W_k, an eyelash is convolved with the wavelet $\varphi_{s(k)}(i) - \varphi_{s(k-1)}(i)$, which has large value at $i = 0$ and decreases as $|i|$ become large. Based on this fact, the weighting value $\omega(i)$ is defined as

$$\omega(i) = 1 - \varphi_{s(k)}(i - c) - \varphi_{s(k-1)}(i - c), \quad i \in \text{nbhd}(c)$$

where c denotes a detected iris location and $\text{nbhd}(c)$ is the neighborhood of the location, c. To reduce the computation time, the weighting values in a small window are precomputed offline.

4.2. Separate Estimation of Signal Rotation Due to Head Tilt

Each one-dimensional intensity signal in the angular direction rotates due to head tilt. Since the rotation value is unknown, we compute the normalized cross-correlation coefficient between two signals by shifting one signal pixel by pixel and choose the shift value that yields the largest cross-correlation coefficient. This method compute the similarity correctly, but makes the similarity between different irises increase.

In the proposed method, we separately estimate the shift amount using the signal at the level zero that is

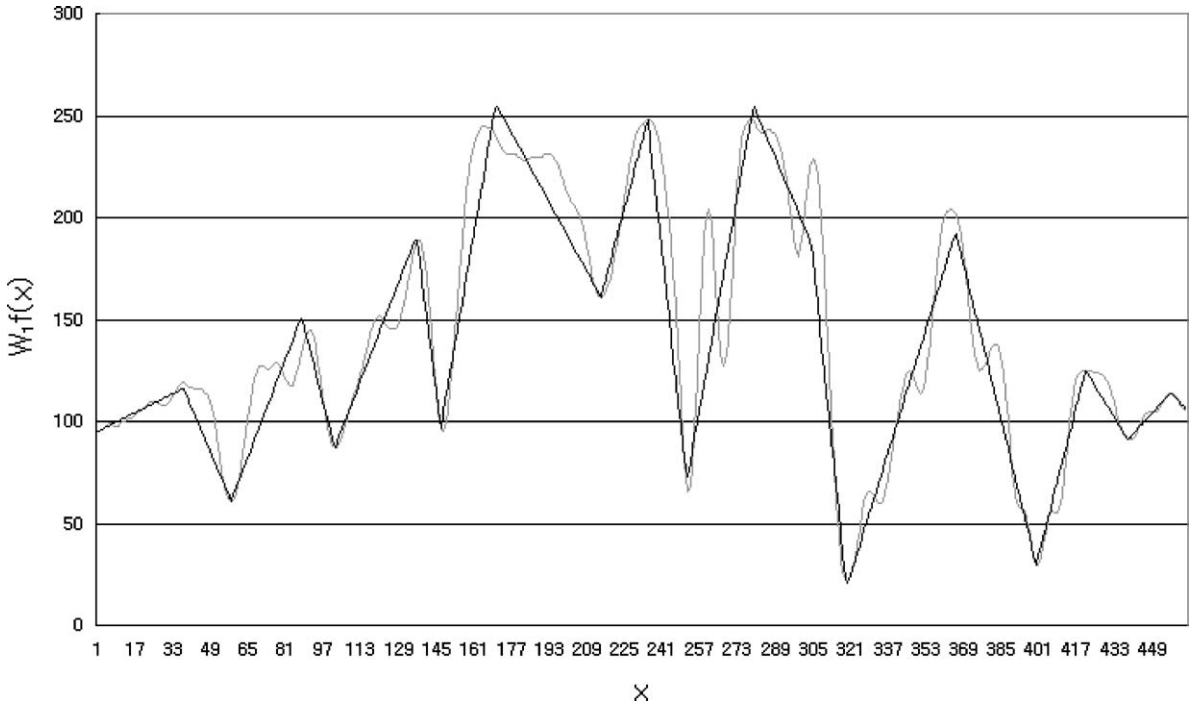

Figure 5. One-dimensional signal in a wavelet domain W_k and the approximated piecewise linear curve.

not used for the similarity measure. This method does not increase the similarity between samples of different irises. The estimated shift value is used in the computation of the cross-correlation coefficients between components at higher levels as follows:

$$\overline{\langle u_{1,\hat{s}}, u_2\rangle} = \frac{\langle u_{1,\hat{s}} \cdot u_2\rangle - \langle u_1\rangle\langle u_2\rangle}{\sigma(u_1)\sigma(u_2)} \quad \text{where}$$
$$\langle u_{1,\hat{s}} \cdot u_2\rangle = \frac{1}{N}\sum_{i=1}^{N} u_1(i+\hat{s})u_2(i). \tag{8}$$

In (8), $\hat{s}$ is the estimated rotation value.

4.3. Classification

We choose the well-known 1-nearest neighbor (1-NN) classification algorithm. Given a training set T and an unknown pattern y_q, 1-NN assigns y_q to the class, which the pattern $y_p \in T$ such that

$$y_p = \arg\max_{y_q \in T} sd(y_p, y_q), \tag{9}$$

belongs to. In (9), $sd(y_p, y_q)$ is the similarity between two samples y_q and y_p.

5. Comparison with Conventional Methods

5.1. Comparison with a Zero-Crossing Method

Zero-crossing points [4, 10] keep information about location of the local maximum and minimum points of each lowpass signal and its local variation. Similarity measures between two corresponding zero-crossing points are robust to a white Gaussian noise. The primary problem of the zero-crossing method is the fact that two representations to be compared can have different numbers of zero-crossings, and some zero-crossing pairs used in computing the similarity may not be corresponding pairs in practical applications. To circumvent the problem, Roche et al. [4] use a binary Hamming distance between two nearest zero-crossing points under the assumption that if two samples are acquired from an identical iris, the distances between corresponding pairs of zero-crossing in one sample and another are less than given threshold value. However, the spurious zero-crossing points can degrade the performance.

In this paper, each decomposed signal is approximated by the optimal piecewise linear curve, and the similarity measure is the normalized cross-correlation

coefficient between the optimally approximated curves. This method makes the iris recognition robust to the spurious zero-crossing points because of two reasons: First, the optimal curve simplification preserves dominant waveform of the signal and filters out a fine details including zero-crossing points. Second, the normalized cross-correlation is less sensitive to the spurious signal variation.

The code size of the two methods are similar because the number of node points is equal to the number of dominant local maximum or minimum points. As for the computation time, the presented method takes less computation times than the zero-crossing method using binary Hamming distance measure. The proposed method requires linear interpolation operations and the zero-crossing method of Roche et al. requires search operations.

5.2. *Comparison with the Method Proposed by Wildes et al.*

In the method of Wildes et al. [2], a Laplacian pyramid [13] is first constructed. Differences between consecutive resolution levels of the Laplacian pyramid serve as the basis for subsequent processing. This method effectively extracts dominant waveform variation in the radial and angular directions. Since two-dimensional bands are used, coarse quantization is required for a compact code size. Similarity measurements in four frequency bands are effectively combined using Fisher's linear discriminant. The highest resolution band is sensitive to noise. The lowest resolution band can be sensitive to head tilt because difference between consecutive levels of the Laplacian pyramid is not translation-invariant [7, 8].

In this paper, the wavelet components of the two-dimensional iris image, robust to noises and containing rich information for iris recognition, are extracted using a continuous wavelet transform that is translation invariant. Since the wavelet components are the low frequencies in the radial direction and the low-mid frequencies in the angular direction, the disc-shaped iris image is first convolved with a low pass filter along the radial direction. Then, the smoothed iris image is decomposed in the angular direction using a one-dimensional continuous wavelet transform. Finally, the optimal approximation procedure reduces the feature vector size while maintaining recognition accuracy.

6. Experiment Results

6.1. *Segmentation Results*

A typical intensity distribution and its estimation using EM are shown in Fig. 1(a). Three segmentation regions processed by a morphological operation with a 5×5 window is shown in Fig. 1(b). The eyelashes, detected using five directional windows, are shown in Fig. 1(c). The segmented pupillary boundary has some error due to the eyelashes. This error is corrected by using the well-known parametric shape modeling method. Figure 1(d) shows the detected pupillary and limbic boundaries.

6.2. *Verification and Classification Results*

As for feature extraction, each signal is analyzed into two components: the lowest resolution level, $L_{s(0)} * g(i, \cdot)$, and the next band, W_1. In our experiments, the lowest level is used for estimating the shift amount of the signal due to the head tilt and the next level is used for computing the normalized correlation coefficients. Since iris images used in the experiments are corrupted by noises, the use of high frequency components does not improve performance.

Finally, we compared the presented iris recognition method with the pyramid decomposition method of Wildes et al. [2] and the zero-crossing method of Martin-Roche et al. [4]. In the implementation of the zero-crossing method, we experimentally found the best threshold value for computing the Hamming distance. In the implementation of the Laplacian pyramid method, we experimentally found the set of resolution levels that yields the best performance because the highest resolution level is sensitive to noises.

The iris database used in the experiments consists of 40 different eyes and, 3 photos per each eye. The photographs were taken in different conditions. Distribution of similarity measures, computed with three different methods, from all possible 14400 comparisons between different pairs of irises in the database are shown in Fig. 6. The distributions of similarity measures between samples of identical irises are illustrated with black bars. The distributions of similarity degrees between samples of different irises are illustrated with gray bars. For the successful verification, the similarity measures between samples of identical

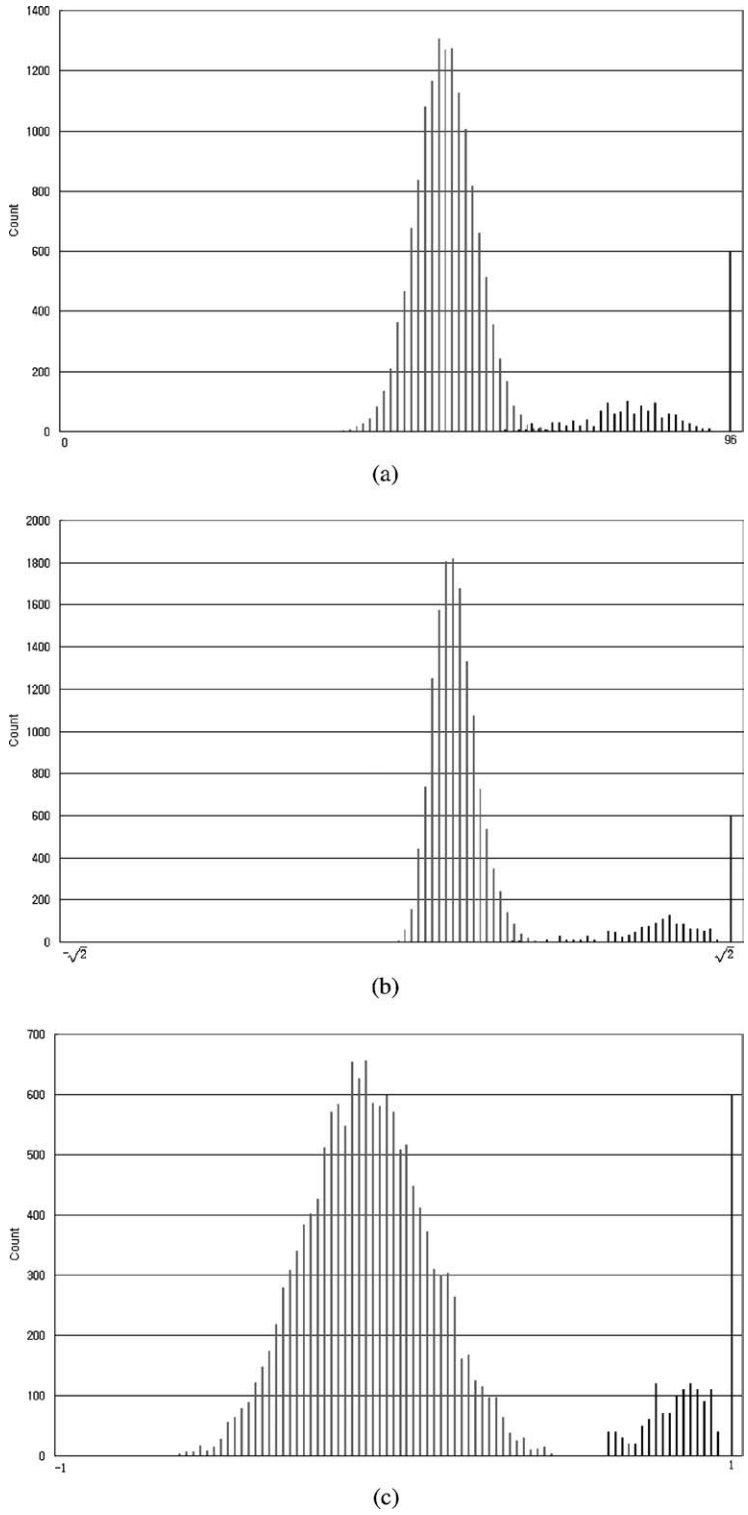

Figure 6. Similarity measures between samples of identical irises and similarity measures between samples of different irises: (a) The zero-crossing method, (b) the pyramid decomposition method and (c) the proposed method. For the illustration, the black bars are at five times the scale of the light bars.

Table 1. Classification accuracies of three methods.

Method	Classification accuracy
Zero-crossing	98.3
Pyramid decomposition	99.4%
The proposed method	100%

irises should be overlapped as less as possible with those between samples of different irises. Figure 6(a) shows the results of the zero-crossing method. Two distributions overlapped by 2.5%. Figure 6(b) shows the results of the pyramid wavelet decomposition method. Two distributions overlapped by 1.0%. Figure 6(c) is the result of the proposed method. Two distributions are separated by a large margin. Table 1 shows the classification accuracies of three different methods. All methods use the 1-NN classification. The proposed method yields the best classification accuracy. The experimental results show that the proposed method outperforms the conventional methods.

7. Conclusion

We have presented a new feature representation method for the iris recognition, which is robust to noises. The disc-shaped iris is first localized. The localized image is convolved with a low pass filter along the radial direction. The radially smoothed iris image is decomposed in the angular direction using a one-dimensional continuous wavelet transform. Each decomposed one-dimensional waveform in the angular direction is represented by an optimal piecewise linear curve connecting a small set of node points. The set of node points is a feature vector to be stored. Experimentally we showed that the proposed method produces superb performance in iris recognition.

Acknowledgment

This work was supported by 2003 Hongik University Research Fund.

References

1. F.H. Adler, *Physiology of the Eye*, St. Louis, MO: Mosby, 1965.
2. R.P. Wildes, "Iris Recognition: An Emerging Biometric Technology," *Proceedings of the IEEE*, vol. 85, 1997, pp. 1348–1363.
3. J. Daugman, "High Confidence Visual Recognition of Person by a Test of Statistical Independence," *IEEE Trans. Pattern Analysis and Machine Intelligence*, vol. 15, 1993, pp. 1148–1161.
4. D. de Martin-Roche, C. Sanchez-Avila, and R. Sanchez-Reillo, "Iris Recognition for Biometric Identification Using Dyadic Wavelet Transform Zero-Crossing," *Security Technology, 2001 IEEE 35th International Carnahan Conference*, 2001, pp. 272–277.
5. Y. Zhu, T. Tan, and Y. Wang, "Biometric Person Identification Based on Iris Pattern," *ICPR2000*, 2000, pp. 805–808.
6. S. Cho and H.I. Sung, "Wavelet Transform and Competitive Learning Neural Network with Multi-Dimensional Wiener Decision Strategy," *Proceeding of KFIS Conference*, vol. 8, no. 2, 1998, pp. 341–345.
7. E.P. Simoncelli, W.T. Freeman, E.H. Adelson, and D.J. Heeger, "Shiftable Multiscale Transforms," *IEEE Trans. Inform. Theory*, vol. 38, 1992, pp. 587–607.
8. S. Mallat, "Wavelets for a Vision," *Proceedings of IEEE*, vol. 84, no. 4, 1996, pp. 604–614.
9. S. Mallat and S. Zhong, "Characterization of Signals from Multiscale Edges," *IEEE Trans. Pattern Analysis and Machine Intelligence*, vol. 14, 1992, pp. 710–732.
10. W.W. Boles and B. Boashah, "A Human Identification Technique Using Images of the Iris and Wavelet Transform," *IEEE Trans. on Signal Processing*, vol. 46, 1998, pp. 1185–1188.
11. J. Li and A. Barron, "Mixture Density Estimation," in *Advances in Neural Information Processing Systems*, Solla, Leen and Mueller (Eds.), vol. 12, The MIT Press, 2000.
12. M. Sonka, V. Hlavac, and R. Boyle, *Image Processing Analysis and Machine Vision*, PWS Publishing, 1999.
13. P.J. Burt and E.H. Adelson, "The Laplacian Pyramid as a Compact Image Code," *IEEE Trans. on Communications*, April 1983, pp. 532–540.

Jaemin Kim received the B.S. and M.S. degrees in electrical engineering from Seoul National University, Korea in 1984 and 1986, respectively. He received the Ph.D. degree in electrical engineering from Rensselaer Polytechnic Institute in 1994. Since 2001, he has been with the School of electronics and electrical engineering, Hongik University, Seoul, Korea, where he is currenltly associate professor. His research interests are biometrics, bioinfomatrics, and image and video processing.
jaemin@hongik.ac.kr

Soengwon Cho received the B.S. degree in electrical engineering from Seoul National University, Korea in 1982. He received the M.S. and Ph.D. degrees in electrical engineering from Purdue University in 1987 and 1992, respectively. He is with Hongik University, Seoul, Korea as an associate professor at School of electronics and electrical engineering. His research interests are biometrics, artificial intelligence, and pattern recognition.
swcho@hongik.ac.kr

Jinsu Choi received the B.S. and M.S. degrees in electrical engineering from the Hongik University, Korea, in 2002 and 2004. He was a Research Assistant at Artificial Intelligence Laboratory in Hongik University from 2002 to 2004. Recently, he is working for the Samsung Electronics Co., Ltd. His research interests are biometrics, especially iris recognition, and artificial intelligence.
jinsus@empal.com

Robert J. Marks II (Ph.D) holds the position of Distinguished Professor of Electrical and Computer Engineering at Baylor University, Waco, TX. He specializes in applied computational intelligence and image inteloligence. Prof. Marks was awarded the Outstanding Branch Councilor award by IEEE and was presented with the IEEE Centennial Medal. He was named a Distinguished Young Alumnus of Rose-Hulman Institute of Technology and is an inductee into the Texas Tech Electrical Engineering Academy. In 2000, he was awarded the Golden Jubilee Award by the IEEE Circuits and Systems Society.

He is Fellow of both IEEE and The Optical Society of America. Dr. Marks serves as an IEEE Distinguished Lecturer. Dr. Marks has over 250 publications. Some of them are very good. Nine of Dr. Marks' papers have been reproduced in volumes of collections of outstanding papers. He has three US patents in the field of artificial neural networks and signal processing. His books include *Neural Smithing: Supervised Learning in Feedforward Artificial Neural Networks* (MIT Press, Cambridge, MA, 1999—with Russell D. Reed.) and R.J. Marks II, *Introduction to Shannon Sampling and Interpolation Theory* (Springer-Verlag, 1991). He is the editor or co-editor of five other volumes. Dr. Marks served as the faculty advisor to the University of Washington's chapter of Campus Crusade for Christ for fifteen years.
r.marks@ieee.org